

# Diffusion, capture and recycling of SCAR/WAVE and Arp2/3 complexes observed in cells by single-molecule imaging

Arthur Millius<sup>1</sup>, Naoki Watanabe<sup>2</sup> and Orion D. Weiner<sup>1,\*</sup>

<sup>1</sup>Cardiovascular Research Institute and Department of Biochemistry, University of California, San Francisco, CA 94158, USA

<sup>2</sup>Laboratory of Single-Molecule Cell Biology, Tohoku University Graduate School of Life Sciences, 6-3 Aoba, Aramaki-Aza, Aoba-ku, Sendai, Miyagi 980-8578, Japan

\*Author for correspondence ([orion.weiner@ucsf.edu](mailto:orion.weiner@ucsf.edu))

Accepted 25 October 2011

Journal of Cell Science 125, 1165–1176

© 2012. Published by The Company of Biologists Ltd

doi: 10.1242/jcs.091157

## Summary

The SCAR/WAVE complex drives lamellipodium formation by enhancing actin nucleation by the Arp2/3 complex. Phosphoinositides and Rac activate the SCAR/WAVE complex, but how SCAR/WAVE and Arp2/3 complexes converge at sites of nucleation is unknown. We analyzed the single-molecule dynamics of WAVE2 and p40 (subunits of the SCAR/WAVE and Arp2/3 complexes, respectively) in XTC cells. We observed lateral diffusion of both proteins and captured the transition of p40 from diffusion to network incorporation. These results suggest that a diffusive 2D search facilitates binding of the Arp2/3 complex to actin filaments necessary for nucleation. After nucleation, the Arp2/3 complex integrates into the actin network and undergoes retrograde flow, which results in its broad distribution throughout the lamellipodium. By contrast, the SCAR/WAVE complex is more restricted to the cell periphery. However, with single-molecule imaging, we also observed WAVE2 molecules undergoing retrograde motion. WAVE2 and p40 have nearly identical speeds, lifetimes and sites of network incorporation. Inhibition of actin retrograde flow does not prevent WAVE2 association and disassociation with the membrane but does inhibit WAVE2 removal from the actin cortex. Our results suggest that membrane binding and diffusion expedites the recruitment of nucleation factors to a nucleation site independent of actin assembly, but after network incorporation, ongoing actin polymerization facilitates recycling of SCAR/WAVE and Arp2/3 complexes.

**Key words:** Actin cytoskeleton, SCAR/WAVE complex, Diffusion, Retrograde flow, Single-molecule imaging

## Introduction

Cells use actin nucleators such as the Arp2 and Arp3 (Arp2/3) complex to control the spatial and temporal dynamics of actin assembly. Activation of the Arp2/3 complex requires its association with actin filaments as well as nucleation-promoting factors such as the SCAR/WAVE complex (Mullins et al., 1998; Machesky and Insall, 1998; Machesky et al., 1999; Rohatgi et al., 1999). Similarly, the SCAR/WAVE complex requires multiple upstream activators such as plasma-membrane-associated phosphoinositides and Rac (Miki et al., 1998; Steffen et al., 2004; Oikawa et al., 2004; Lebensohn and Kirschner, 2009; Chen et al., 2010). Proteins in the SCAR/WAVE family are essential for actin polymerization and movement in many different cell contexts (Bear et al., 1998; Miki et al., 1998; Zallen et al., 2002; Yan et al., 2003; Rogers et al., 2003; Weiner et al., 2006; Ibarra et al., 2006; Patel et al., 2008).

The Arp2/3 complex and other actin regulators associate with the actin network, which is pushed away from the leading edge of a cell in a process called retrograde flow. Retrograde flow was first visualized with techniques such as FRAP and photoactivation (Wang, 1985; Theriot and Mitchison, 1991; Theriot and Mitchison, 1992; Lin and Forscher, 1995; Cramer and Mitchison, 1997). Because data from these techniques can hide local differences in actin assembly, researchers have recently used additional methods such as single-molecule and speckle microscopy to analyze

the fine-grained spatial and temporal dynamics of actin rearrangements (Watanabe and Mitchison, 2002; Ponti et al., 2004). Single-molecule imaging has also been used to study actin-associated proteins such as the Arp2/3 complex and capping protein, which have different lifetimes in the actin network (Ponti et al., 2005; Miyoshi et al., 2006; Iwasa and Mullins, 2007). However, single-molecule imaging has not been applied to nucleation-promoting factors such as the SCAR/WAVE complex, and it is unknown whether the SCAR/WAVE complex incorporates into the actin network.

Imaging in other non-single-molecule modes shows that the SCAR/WAVE complex is recruited to the edge of the lamellipodium in fibroblasts (Stradal et al., 2001; Lai et al., 2008) and propagates in ‘waves’ of actin assembly at the leading edge of neutrophils and *Dictyostelium* (Weiner et al., 2007; King et al., 2010; Xiong et al., 2010). However, these imaging modes might obscure molecules whose dynamics differ from the global population. To elucidate mechanisms of recruitment of the SCAR/WAVE complex to the plasma membrane, convergence with the Arp2/3 complex on a membrane-apposed actin filament, and removal from the membrane, we analyzed the single-molecule dynamics of WAVE2 in *Xenopus* tissue culture (XTC) cells. In addition to its peripheral association with the leading edge, we show that WAVE2 molecules incorporate into the growing lamellipodial actin network. WAVE2 undergoes

retrograde flow at similar speeds, sites of initiation, and lifetimes to that of actin and the p40 subunit of the Arp2/3 complex. Using a drug cocktail that stabilizes the existing cytoskeleton while blocking new assembly, we demonstrate that ongoing actin polymerization is not required for WAVE2 association and dissociation with the membrane, but is required for removal of WAVE2 from the cortex. Finally, we show that p40 and WAVE2 laterally diffuse in the membrane and capture the transition of p40 from lateral diffusion to network incorporation. Based on these data, we propose that the SCAR/WAVE and Arp2/3 complexes locally search the membrane before converging on sites of actin nucleation, and are removed from the actin network through the force of retrograde flow.

## Results

### Single-molecule imaging shows that WAVE2 undergoes retrograde flow in XTC cells

We used a crippled CMV promoter to express the low concentration of WAVE2–GFP that is required for single-molecule imaging. Because XTC cells have flat protrusions, single molecules can be visualized with epifluorescence microscopy. This enabled us to image thicker sections than can be achieved with TIRF and with less photodamaging light than needed for confocal imaging. Long camera exposures

enabled us to view stabilized fluorescent probes attached to the membrane or cytoskeleton while blurring fast diffusing molecules (Watanabe and Mitchison, 2002). Under these imaging conditions, we observed WAVE2–EGFP molecules in the lamellipodium, filopodia, and regions near the lamellipodium interior (Fig. 1A, left), which is consistent with the known overall distribution of WAVE2 in non-single-molecule imaging mode (Hahne et al., 2001; Stradal et al., 2001; Lai et al., 2008). Surprisingly, we observed persistent movement of WAVE2 molecules away from the leading edge (Fig. 1 and supplementary material Movie 1). Kymograph analysis revealed that retrograde motion of WAVE2 was smooth and continuous (Fig. 1A, left, inset). WAVE2 retrograde movement can be visualized with a maximum intensity projection over the course of the epifluorescence acquisition (Fig. 1A, middle). Here, retrograde motion appeared as linear streaks, as indicated by the arrows. WAVE2–EGFP molecules with retrograde motion had a unimodal distribution of intensities that was similar to p40–EGFP and GFP–actin single molecules and photobleach in a single step (supplementary material Fig. S1). Therefore, these retrograde movement events are likely to represent single molecules. Retrograde flow of WAVE2 was more difficult to observe with shorter exposures in TIRF microscopy (supplementary material Fig. S2A), because transient recruitment of WAVE2 obscures stabilized pools of

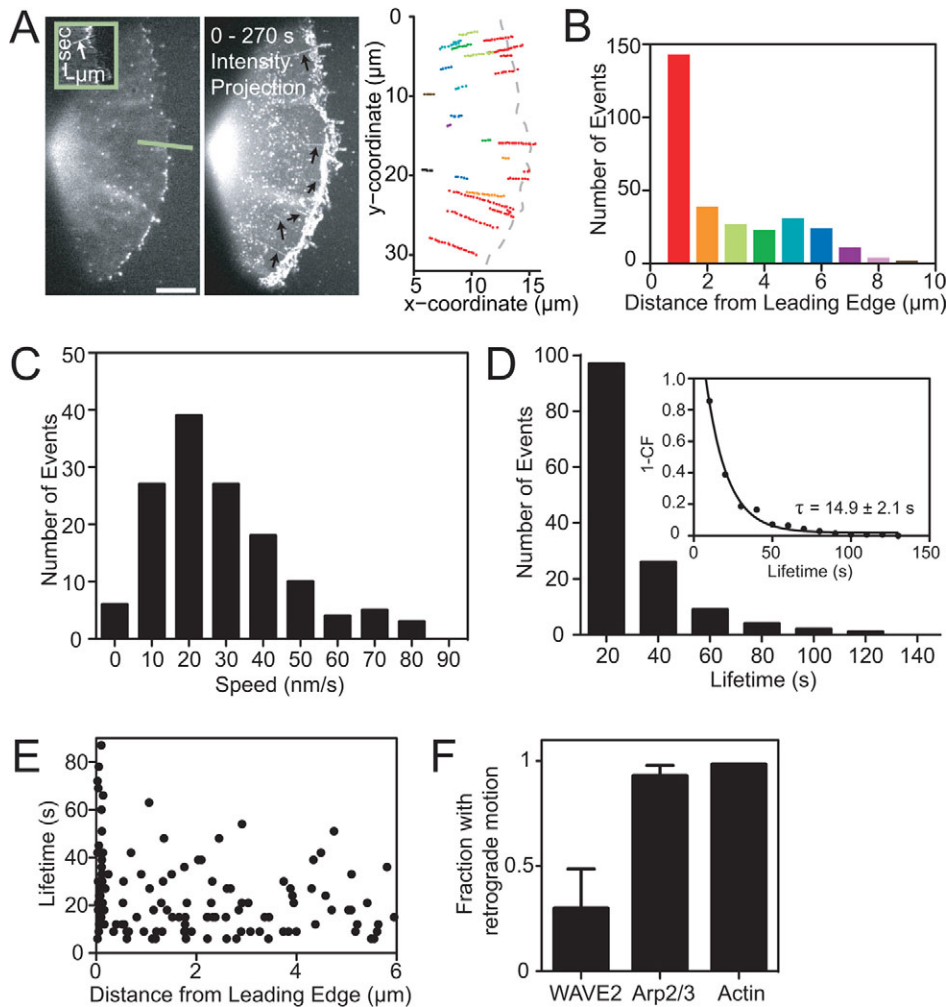


**Fig. 1. Single-molecule epifluorescence imaging demonstrates retrograde flow of WAVE2 in XTC cells.** (A) Fluorescence image (left) of an XTC cell expressing a low concentration of WAVE2–EGFP. Some molecules undergo smooth and continuous retrograde flow (inset, kymograph bars: horizontal, 1  $\mu\text{m}$ ; vertical, 1 min; time flows top to bottom). Middle panel shows maximum intensity projection (90 frames, 4.5 minutes) of this cell. Arrows indicate retrograde flow events. Corresponds to supplementary material Movie 1. Trajectories of retrograde flowing molecules are shown on the right. Color corresponds to histogram in B and indicates the distance to the leading edge when the molecule first appears. Scale bar: 5  $\mu\text{m}$ . (B) Initial positions of appearance for retrograde WAVE2 molecules as a function of distance from the leading edge ( $n=304$ , nine cells). (C) Distribution of WAVE2 retrograde velocities with a mean speed of  $31 \pm 18$  nm/second ( $n=345$ , nine cells). (D) Lifetime distribution of WAVE2 molecules ( $n=345$ , nine cells) that appear over the course of a 90 second time window. Single exponential fit of 1-cumulative frequency (CF) of WAVE2 lifetimes gives a mean lifetime ( $\tau$ ) of  $14.9 \pm 2.1$  seconds (inset). (E) Lifetime versus position plot for WAVE2 molecules. Dots represent the lifetime and emerging position of individual WAVE2 molecules ( $n=143$ , six cells). (F) Fraction of fluorescent WAVE2 (19%,  $n=1810$ , nine cells), p40 (93%,  $n=3068$ , three cells), and actin (98%,  $n=4503$ , three cells) molecules undergoing retrograde flow. Error bars are s.d.

WAVE2 on the plasma membrane and/or cytoskeleton. We also observed retrograde movement with another subunit of the WAVE complex, Abi-EGFP (supplementary material Fig. S2B and Movie 2), supporting the idea that retrograde movement of WAVE2 and Abi reflect the movement of the SCAR/WAVE complex as a whole. Most of our experiments were performed on polylysine, but we also observed WAVE2 retrograde motion on more physiological substrates such as fibronectin, which reduced the retrograde flow speed of WAVE2 (supplementary material Fig. S2C,D). Under these conditions, integrin coupling to fibronectin probably slows actin retrograde flow velocity, which is consistent with earlier reports (Renkawitz et al., 2009).

Cells spatially bias actin polymerization to control shape and movement. The appearance of both actin and p40 is strongly biased toward the leading edge (Watanabe and Mitchison, 2002; Miyoshi et al., 2006). Similarly, the initial position of appearance for retrograde moving molecules of WAVE2 was biased to within 1  $\mu\text{m}$  of the leading edge (Fig. 1A, right and Fig. 1B), suggesting that most actin assembly mediated by the SCAR/WAVE complex occurs in this region. Molecules of WAVE2 that had undergone retrograde flow had a mean speed of 31 nm/second (Fig. 1C). The distribution of WAVE2 lifetimes was well fit by a single exponential curve with a mean lifetime ( $\tau$ ) of  $14.9 \pm 2.1$  seconds (Fig. 1D and inset). We could not measure speed and lifetime for WAVE2 molecules that stayed on the cell edge because individual molecules were not resolvable. Our single-molecule lifetime measurements were roughly similar to lifetimes measured with population techniques (Fig. 4F) (Weiner et al., 2007; Lai et al., 2008). We observed no spatial bias in the lifetime of WAVE2 molecules as a function of the distance from the leading edge where they first appeared (Fig. 1E), which was similar to a lifetime versus position plot for Arp2/3 (Miyoshi et al., 2006).

### Actin and p40 retrograde flow are similar to WAVE2 retrograde flow

Because the site of appearance and speed of retrograde flow for WAVE2 molecules are similar to actin retrograde flow, we hypothesized that the SCAR/WAVE complex might be hitchhiking with the Arp2/3 complex on the retrograde-flowing network. To gain greater insight into the relative dynamics of the SCAR/WAVE complex, the Arp2/3 complex, and actin, we compared their rates of retrograde flow and lifetimes in the actin network. Observation of the GFP-tagged p40 subunit of the Arp2/3 complex (Fig. 2A and supplementary material Movie 3) demonstrated that p40 had a remarkably similar mean retrograde flow speed of 30 nm/second (Fig. 2C) to that of WAVE2 (31 nm/second, Fig. 1C). Similarly, the lifetime of p40 during retrograde flow was  $15.2 \pm 0.5$  seconds (Fig. 2E, compared with  $14.9 \pm 2.1$  seconds for WAVE2, Fig. 1D) and did not depend on where molecules initially appeared (supplementary material Fig. S2D). When we observed cells expressing low amounts of EGFP-actin (Fig. 2B and supplementary material Movie 4), we also found that actin had a similar mean retrograde speed of 25 nm/second (Fig. 2D) and a mean lifetime in the network of  $18.4 \pm 0.5$  seconds (Fig. 2F). This is comparable to previous reported values of actin retrograde flow in XTC cells (Watanabe and Mitchison, 2002) but is greater than the mean speed of actin retrograde flow reported in microinjected PtK1 cells using speckle microscopy (Ponti et al., 2004). Similar to WAVE2, the

appearance of p40 and actin molecules was heavily biased to within 1  $\mu\text{m}$  of the leading edge (Fig. 2G,H). The distribution of p40 might be more restricted than either actin or WAVE2 for several reasons: other Arp2/3 complex activators such as WASP or N-WASP in combination with WAVE2 might further bias Arp2/3 to the cell periphery, or undersampling of WAVE2 particles at the periphery might occur because WAVE2 accumulation in that region masks the initial appearance of WAVE2 particles with retrograde motion. These data support a model where SCAR/WAVE and Arp2/3 complexes both incorporate into the actin network, maintain their interaction during retrograde flow, and are dissociated from the network together.

In cells expressing both p40-EGFP and EGFP-actin, all observable molecules underwent retrograde flow. Therefore, a large number of tracks could be collected with few cells. By contrast, WAVE2-EGFP retrograde flow was a comparatively rare event (compare Fig. 2A,B middle panels to Fig. 1A middle panel and quantified in Fig. 1F). We hypothesize that this is because only a subset of SCAR/WAVE complexes participate in Arp2/3 complex recruitment and actin nucleation. This is consistent with the observation that the SCAR/WAVE complex shows a much stronger peripheral association with the lamellipodium than does the Arp2/3 complex.

### Inhibition of retrograde flow impedes recycling of p40

Previously, actin polymer has been shown to be involved in the recycling of the WAVE complex (Weiner et al., 2007) and other nucleation-promoting factors (Weisswange et al., 2009). Furthermore, actin polymer helps to sculpt the spatial distribution of the WAVE complex in response to external stimuli (Millius et al., 2009). However, these experiments relied on treating cells with single pharmacological inhibitors of actin assembly such as the actin-sequestering drug latrunculin. These drugs not only inhibit new polymerisation, but also result in the disassembly of the existing actin network. These dual effects make it difficult to determine whether basal actin polymer or ongoing actin assembly is more relevant for SCAR/WAVE complex recycling. To address this question, we used a three-drug cocktail to stabilize the existing network while preventing new actin polymerization (Peng et al., 2011).

This cocktail involves incubating cells in a mixture of 10  $\mu\text{M}$  Rho kinase inhibitor Y27632 (Y) for 30 minutes to inhibit myosin-II-based actin contraction, then simultaneously adding 20  $\mu\text{M}$  latrunculin (L) to prevent new actin assembly and 20  $\mu\text{M}$  jasplakinolide (J) to stabilize existing actin structures (Fig. 3A). We verified that this JLY drug combination blocks actin nucleation (visualized by retrograde flow of p40-EGFP) and disassembly of the actin network (visualized by the lifetime of p40-EGFP in the actin network). Untreated cells expressing p40-EGFP had significant retrograde flow (trajectories shown in Fig. 3B, left), which is apparent by long streaks in a maximum intensity projection (Fig. 3B, middle) and diagonal lines in the kymograph (Fig. 3B, right). By contrast, p40-EGFP molecules in cells treated with the JLY cocktail remained stably associated with the network; note the lack of long trajectories in drug-treated cells (Fig. 3C, left) and fixed points in the maximum intensity projection (Fig. 3C, middle). The lack of retrograde movement was also apparent as vertical instead of diagonal streaks in the kymograph (Fig. 3C, right). Analysis of trajectories confirmed that retrograde speed decreased (Fig. 3D) and lifetime increased (Fig. 3E) with drug treatment. To test whether our single-molecule measurements

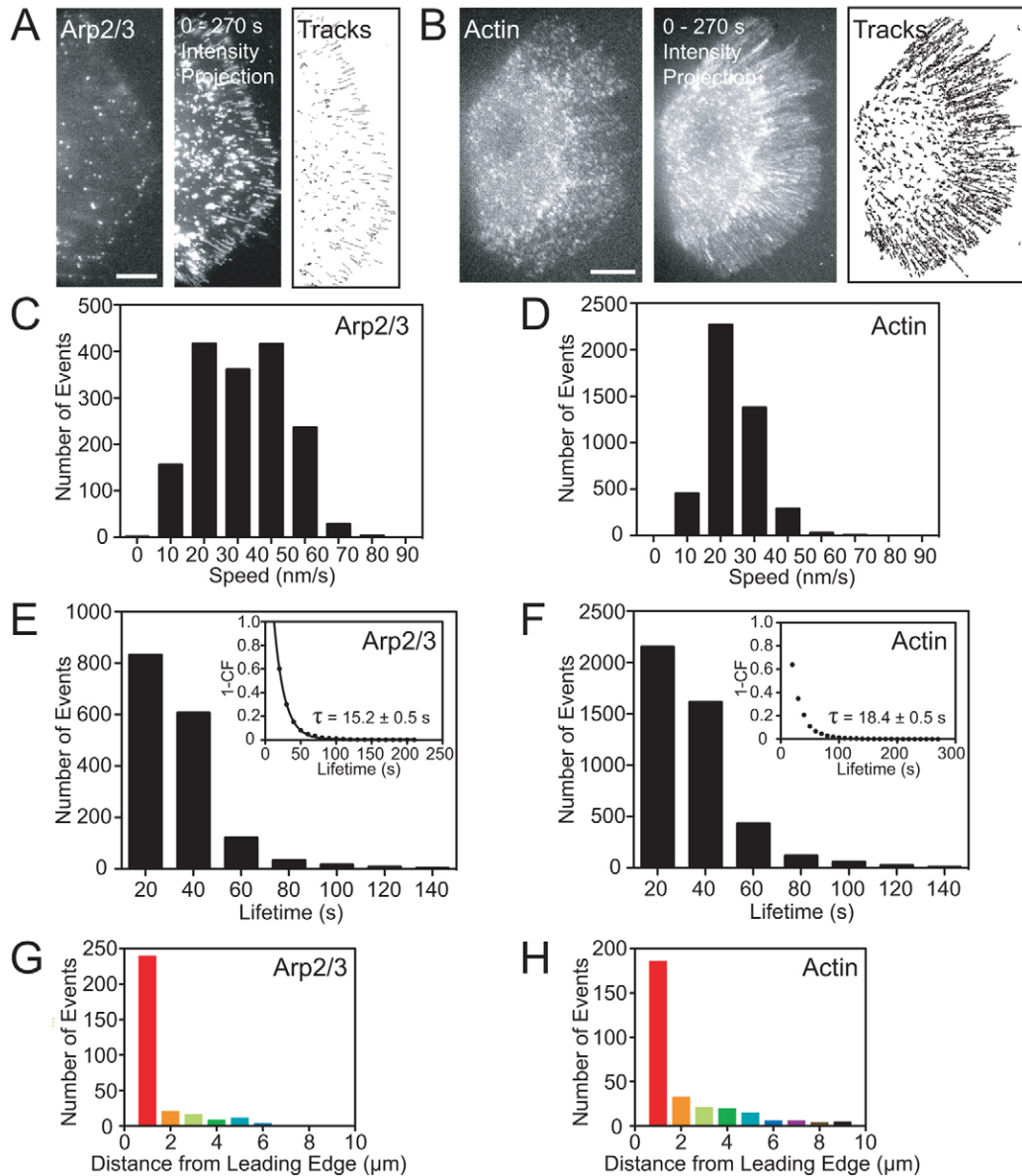


**Fig. 2. Actin and p40 retrograde flow is similar to WAVE2 retrograde flow.** (A) Left panel shows epifluorescence image of an XTC cell expressing a low concentration of EGFP-tagged p40 subunit of the Arp2/3 complex (corresponds to supplementary material Movie 3). Scale bar: 5  $\mu$ m. Middle panel shows maximum intensity projection (90 frames, 4.5 minutes) of this cell, and right panel shows the trajectories of retrograde flowing molecules. (B) Left panel shows fluorescence image of an XTC cell expressing a low concentration of EGFP-actin (corresponds to supplementary material Movie 4). Scale bar: 5  $\mu$ m. Middle panel shows maximum intensity projection (90 frames, 4.5 minutes) of this cell, and right panel shows trajectories of retrograde flowing molecules. (C) Distribution of p40 retrograde velocities with a mean speed of  $30 \pm 13$  nm/second ( $n=1696$ , three cells). (D) Distribution of actin retrograde velocities with a mean speed of  $24 \pm 8$  nm/second ( $n=4503$ , three cells). (E) Lifetime distribution of p40 molecules ( $n=1696$ , three cells) that appear over the course of a 90 second time window. Four speckles had lifetimes longer than 140 seconds; the longest speckle lifetime was 200 seconds. Single exponential fit of 1-CF of p40 lifetimes ( $\tau=15.2 \pm 0.5$  seconds, inset). (F) Lifetime distribution of actin molecules ( $n=4503$ , three cells) that appear over the course of a 90 second time window. Fourteen speckles had lifetimes longer than 140 seconds; the longest speckle lifetime was 280 seconds. Single exponential fit of 1-CF of actin lifetimes ( $\tau=18.4 \pm 0.5$  seconds, inset). (G,H) Initial positions of appearance for retrograde moving p40 (G,  $n=304$ , three cells) and actin (H,  $n=304$ , three cells) molecules as a function of distance from the leading edge.

reflected the global behavior of the actin network, we examined the morphology and bulk p40-EGFP fluorescence of a cell before and after JLY drug application (Fig. 3F and supplementary material Movie 5). Before JLY drug treatment, cell protrusion and retraction led to a difference of  $\sim 8\%$  in the overlapping cell area. By contrast, after drug treatment, the overlapping area was nearly identical (only 1% difference) because the cell had ceased to protrude and retract.

Fluorescence of p40-EGFP also became stabilized after drug addition (Fig. 3F, bottom). We examined p40-EGFP fluorescence recovery after photobleaching (FRAP) to show that new p40-EGFP incorporation in the actin network did not occur (Fig. 4E). Together, these data indicate that the JLY drug cocktail inhibits new actin assembly while stabilizing existing actin structures.

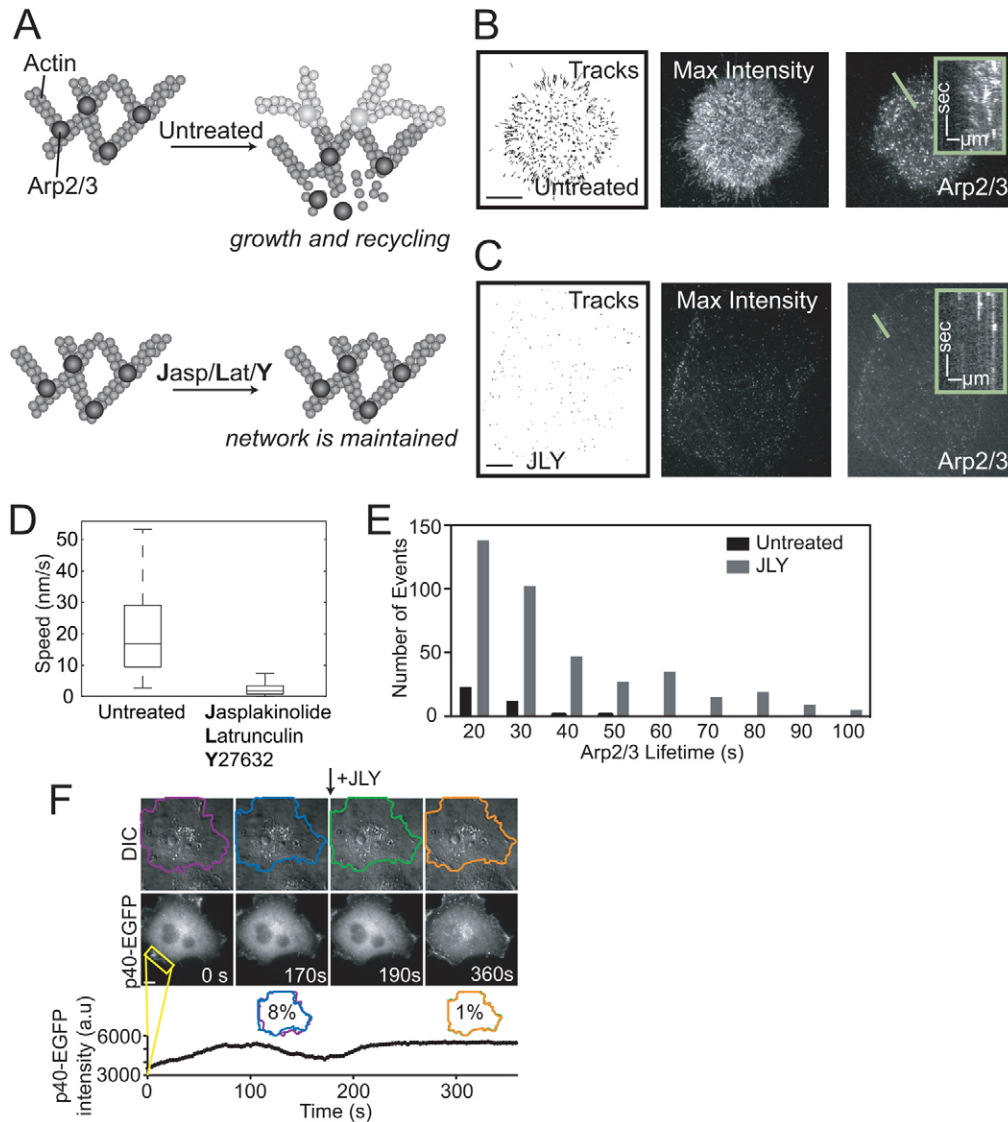


**Fig. 3. p40 recycling depends on actin dynamics.** (A) XTC cells were treated with a drug cocktail that inhibits both actin polymerization and network turnover. Cells were pretreated for 30 minutes with 10  $\mu\text{M}$  Y27632 (Y) and then acutely treated with 20  $\mu\text{M}$  jaspalakinolide (J) and 20  $\mu\text{M}$  latrunculinB (L). Small circles represent actin and large circles represent the Arp2/3 complex. Dark gray shows the existing network, and new network growth is shown in light gray. (B) Left panel shows trajectories of retrograde flowing molecules from an XTC cell expressing a low concentration of p40-EGFP. Middle panel shows maximum intensity projection (90 frames, 4.5 minutes) of this cell, and right panel shows a single TIRF image of the cell. Diagonal streaks in the inset kymograph show most molecules undergo smooth and continuous retrograde flow (inset bars: horizontal, 2  $\mu\text{m}$ ; vertical, 1 minute; time flows top to bottom). Scale bar: 10  $\mu\text{m}$ . (C) Left panel shows trajectories of retrograde flowing molecules from a cell expressing p40-EGFP treated with JLY cocktail described in A. Middle panel shows maximum intensity projection (90 frames, 4.5 minutes) of this cell, and right panel shows a single TIRF image of the cell. Vertical streaks in the inset kymograph indicate that freezing actin dynamics causes p40 to cease retrograde flow (inset bars: horizontal, 2  $\mu\text{m}$ ; vertical, 1 minute; time flows top to bottom). Scale bar: 10  $\mu\text{m}$ . (D) p40 retrograde flow speed is reduced in JLY-treated cells (mean=3 nm/second) compared with untreated cells (mean=18 nm/second), indicating a drug-dependent block of retrograde flow. (E) p40 lifetime increases after drug addition, indicating stabilization of the existing actin network (before,  $n=37$ ; after,  $n=397$ ). (F) An XTC cell expressing p40-EGFP imaged in DIC (top) and GFP (middle) was treated at 180 seconds with JLY cocktail. A section of the lamellipodium (yellow box) was measured for protrusion and retraction over time and the cell boundary was measured at each frame for area of overlap with previous frames (bottom). Percentages inside colored cell traces indicate the difference in overlap between indicated frames. Corresponds to supplementary material Movie 5. Scale bar: 5  $\mu\text{m}$ .

### WAVE2 recycles through actin-dependent and actin-independent mechanisms

To examine how actin regulators depend on ongoing actin polymerization and depolymerization, we analyzed the effect of JLY in cells expressing low levels of p40-EGFP or WAVE2-EGFP, imaged with TIRF microscopy. To visualize the results of

this experiment, we created a kymograph across the whole cell using the 'Reslice' function in ImageJ, which shows how molecules change before and after drug treatment. Then we applied a maximum intensity projection ('Z Project' function in ImageJ) across all kymograph slices to visualize every region of the cell in one frame. After JLY drug treatment, Arp2/3

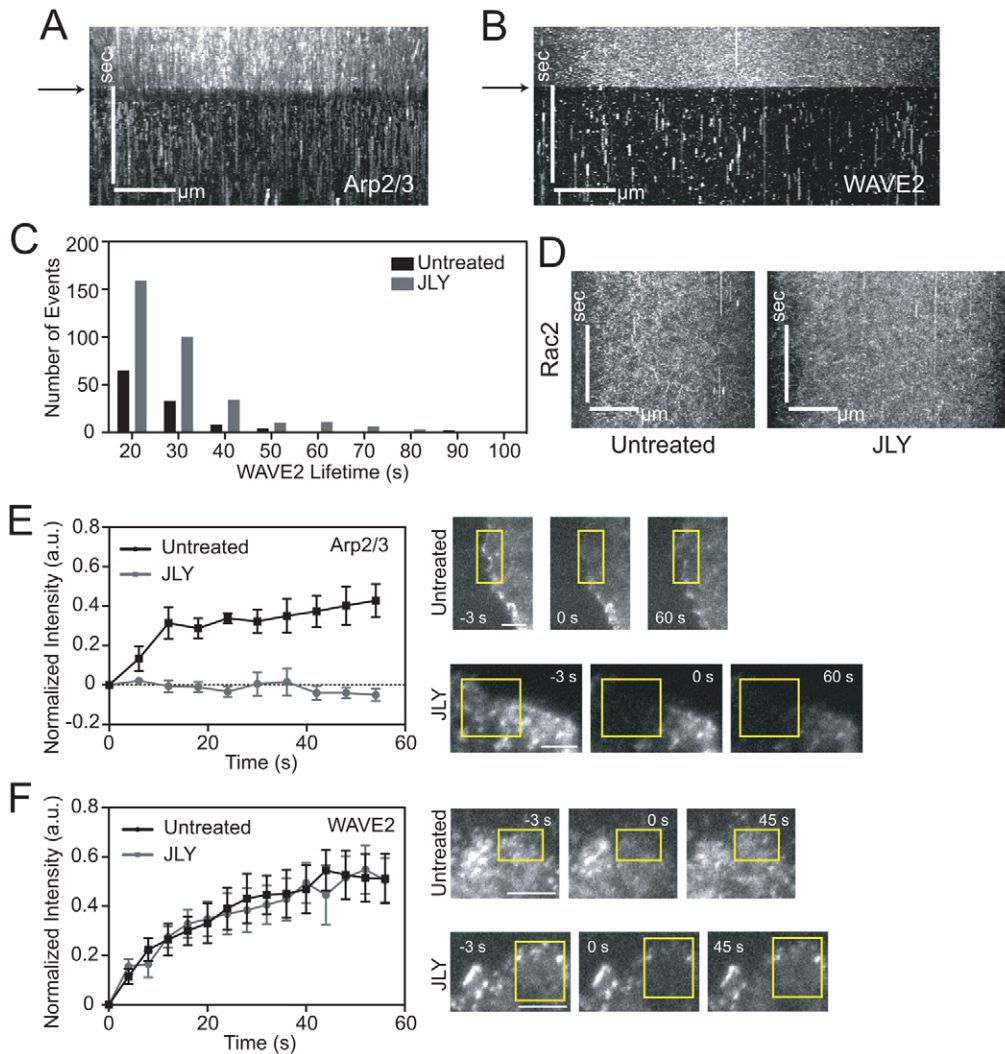


**Fig. 4. WAVE2 freely associates and dissociates with the plasma membrane until incorporation into the actin cortex.** (A,B) Maximum intensity projection (180 frames, 9 minutes) of a kymograph across an XTC cell expressing p40-EGFP (A) or WAVE2-EGFP (B) before and after treatment with JLY drug cocktail. Arrow indicates drug addition. Bars: horizontal, 1  $\mu$ m; vertical, 5 minutes. Time flows top to bottom. Drug treatment stabilizes both p40 and WAVE2 molecules on the membrane, as indicated by vertical streaks at time points below arrow in the kymograph. (C) Lifetime of stabilized WAVE2 molecules increases after drug treatment (before,  $n=113$ ; after,  $n=324$ ). (D) Maximum intensity kymograph projections of XTC cells expressing Rac2-EGFP in the absence or presence of the JLY drug cocktail. Compare with portion of kymograph in Fig. 4B above the black arrow. Bars: horizontal, 1  $\mu$ m; vertical, 5 minutes. Time flows top to bottom. (E,F) FRAP to ascertain how bulk populations of Arp2/3 (E) and WAVE2 (F) behave after actin network stabilization with JLY. Cells were pretreated for 30 minutes with JLY (gray lines) or buffer (black lines). (E) p40-EGFP recovers  $\sim 40\%$  of its pre-bleached fluorescence ( $n=7$ ), whereas cells treated with JLY do not show any recovery ( $n=6$ ). (F) WAVE2-EGFP recovers similarly in both drug-treated ( $n=7$ ) and untreated ( $n=8$ ) cells. Representative images are shown on the right. Yellow rectangles indicate photobleached regions. Scale bars: 2.5  $\mu$ m.

complexes became stabilized (Fig. 4A, long vertical streaks; arrow indicates drug addition). Next, we examined WAVE2-EGFP dynamics after acute inhibition of actin polymerization and depolymerization (Fig. 4B,C). Before drug treatment, most WAVE2 molecules transiently associated with the cell membrane and/or cytoskeleton (Fig. 4B, punctate spots above arrow). After actin dynamics cease, a few WAVE2 molecules remained associated with the membrane and/or cytoskeleton (Fig. 4B, long streaks of WAVE2 below arrow in the kymograph; WAVE2 lifetime is quantified in Fig. 4C). To test for a general perturbation of plasma membrane interactions, we assayed the dynamics of the association of Rac2-GFP with the plasma membrane. Rac2 membrane association was equivalent in the presence and absence of JLY (Fig. 4D) and resembled WAVE2 interaction with the membrane before drug treatment (Fig. 4B, above arrow). These data suggest that a subset of SCAR/WAVE molecules (probably those associated with the cytoskeleton) require ongoing actin polymerization for recycling, which is consistent with the observed WAVE2 retrograde flow. To test whether this actin dependence was similar for all WAVE2 molecules, we assayed the global pool of WAVE2 for

actin-dependent recycling using FRAP. Here, WAVE2-EGFP molecules recovered similarly in both untreated and JLY-treated experiments (Fig. 4F) in contrast to p40-EGFP (Fig. 4E), which suggests that most WAVE2 molecules freely associate and dissociate with the plasma membrane and do not require an actin-nucleation event for membrane dissociation. Together, our data suggest that most WAVE2 molecules interact with the membrane in an actin-independent manner, but once WAVE2 becomes integrated into the actin network (presumably through Arp2/3 activation), actin-dependent retrograde flow is required for WAVE2 turnover.

#### WAVE2 and p40 undergo lateral diffusion similar to membrane-associated proteins

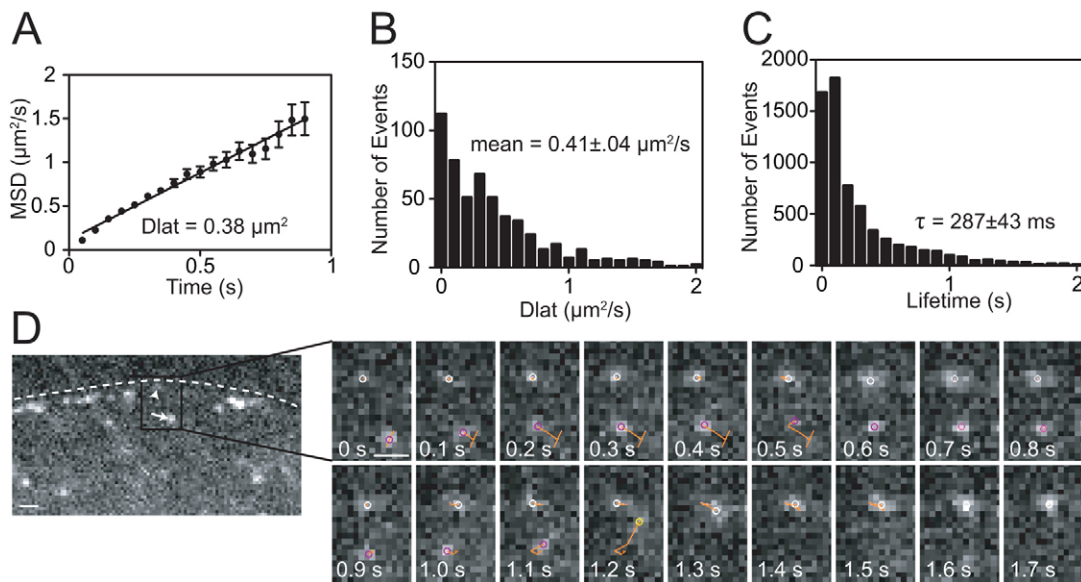
We next sought to address how SCAR/WAVE and Arp2/3 complexes arrive at sites of actin nucleation. Arp2/3 complex activation involves its association with nucleation-promoting factors (such as the SCAR/WAVE complex) as well as an actin filament (Mullins et al., 1998; Machesky et al., 1999). Furthermore, the SCAR/WAVE complex is recruited and activated at membranes by association with phospholipids

and GTP-bound Rac (Lebensohn and Kirschner, 2009; Padrick and Rosen, 2010). How do all of these components converge to one point in space and time for actin nucleation? We envisioned two possibilities: (1) SCAR/WAVE and Arp2/3 complexes are recruited directly from the cytosol to bind a membrane-associated actin filament, or (2) SCAR/WAVE and Arp2/3 complexes diffuse in the plane of the membrane in search of an actin filament. Consistent with the second hypothesis, when we imaged cells expressing low amounts of WAVE2-EGFP in TIRF microscopy at high-temporal resolution, we observed laterally diffusing molecules (supplementary material Movie 6).

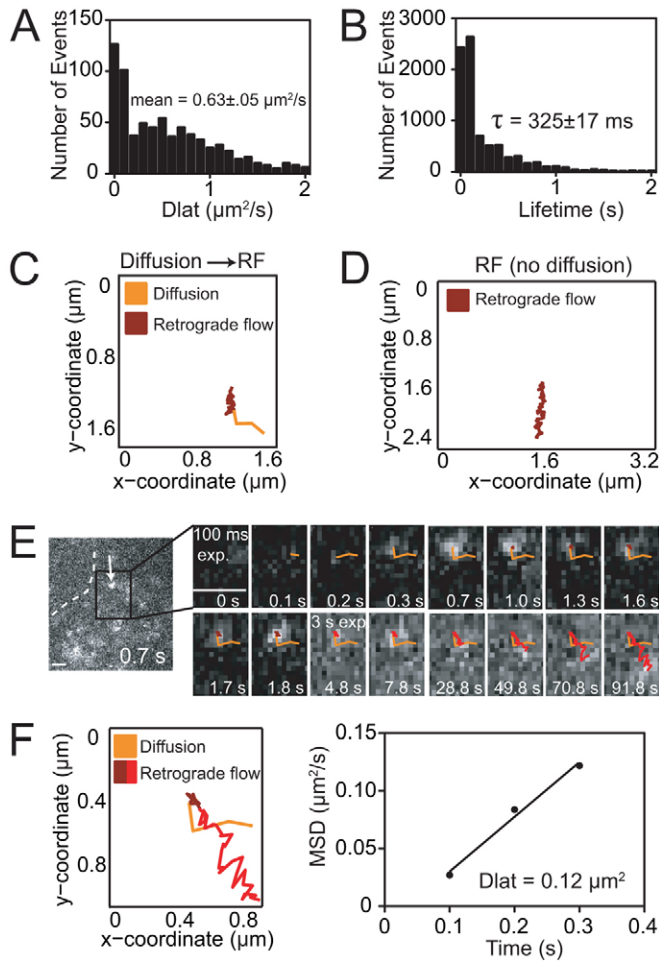
We hypothesized that lateral diffusion of WAVE2 reflects its association with membrane-bound components such as Rac-GTP or phosphoinositides. We used mean-squared displacement (MSD) versus time-lag plots to analyze the diffusion of WAVE2 molecules (a representative plot is shown in Fig. 5A). A histogram of lateral diffusion coefficients gave a mean diffusion constant for WAVE2 of  $0.41 \pm 0.04 \mu\text{m}^2/\text{second}$  (Fig. 5B). This is similar to previous reported values for lateral diffusion of Ras-GFP in the membrane (Murakoshi et al., 2004), and is similar to our own analysis of Rac2-GFP lateral diffusion (supplementary material Fig. S3A,B and Movie 7). Lateral diffusion of WAVE2 was not prevented by the presence of dominant-negative RacN17 (supplementary material Fig. S3C). This is consistent with previous data that the SCAR/WAVE complex has multiple modes of binding to the plasma membrane (Miki et al., 1998; Steffen et al., 2004; Oikawa et al., 2004; Lebensohn and Kirschner, 2009; Chen et al., 2010). We could measure a slight, but statistically significant increase in the mean lateral diffusion coefficient of WAVE2 in the presence of RacN17 ( $0.54 \pm 0.02 \mu\text{m}^2/\text{second}$ , supplementary material Fig. S3C compared with  $0.41 \pm 0.04 \mu\text{m}^2/\text{second}$  in control cells,

Fig. 5B), which suggests that Rac-GTP might limit the diffusion of the SCAR/WAVE complex through direct binding or through mediating the interaction of the SCAR/WAVE complex with downstream signaling events such as association with the actin cytoskeleton. In some cases, we observed WAVE2 transition from lateral diffusion to immobilization (a representative cell is shown in Fig. 5D, and supplementary material Movie 8), possibly representing a precursor to retrograde flow. We also observed p40-EGFP diffusion (Fig. 6 and supplementary material Movie 9) with a mean diffusion constant of  $0.63 \pm 0.06 \mu\text{m}^2/\text{second}$  (Fig. 6A). WAVE2 and p40 also have similar residence times on the membrane ( $\tau = 287 \pm 43$  mseconds Fig. 5C and  $\tau = 325 \pm 17$  mseconds Fig. 6B, respectively). Our data support a model where the Arp2/3 complex binds the SCAR/WAVE complex and diffuses along the membrane in search of an actin filament for Arp2/3 complex activation.

Are laterally diffusing Arp2/3 complex molecules precursors to actin nucleation? To address this question, we performed extended high-speed imaging of cells that contained both stationary and diffusing p40-EGFP molecules. We observed individual particle diffusion before retrograde flow (an example is shown in Fig. 6C and supplementary material Movie 10), although not all retrograde flow events were preceded by detectable lateral diffusion (Fig. 6D and supplementary material Movie 11). In this high-intensity rapid imaging mode, molecules photobleached rapidly, which made it difficult to discern retrograde motion from an immobile particle. To better capture the transition from lateral diffusion to retrograde flow, we switched imaging frequencies during the acquisition. We first imaged molecules in a high-frequency mode to capture lateral diffusion and then switched to a low-frequency, low-light mode that is more optimal to observe retrograde flow for long periods



**Fig. 5. WAVE2-EGFP molecules diffuse at rates consistent with membrane diffusion.** (A) An example of a MSD versus time lag plot for all diffusing particles in a cell expressing WAVE2-EGFP gives a mean lateral diffusion coefficient of  $0.38 \mu\text{m}^2/\text{second}$  (corresponds to supplementary material Movie 6). Error bars are s.e.m. (B) Histogram of WAVE2 lateral diffusion coefficients for particles that diffuse at least 20 frames ( $n=543$ , five cells) with mean diffusion coefficient of  $0.41 \pm 0.04 \mu\text{m}^2/\text{second}$ . (C) Lifetime distribution of diffusing WAVE2 molecules ( $n=6647$ , five cells). Single exponential fit of 1-CF (not shown) gives a mean lifetime of  $287 \pm 43$  mseconds. (D) Representative time-lapse image sequence of a WAVE2-EGFP molecule (arrow) diffusing and then stabilizing at the leading edge (arrowhead indicates stabilization point; corresponds to supplementary material Movie 8). Dashed line indicates cell edge. Scale bars:  $1 \mu\text{m}$ .



**Fig. 6. The Arp2/3 complex transitions from lateral diffusion to retrograde flow.** (A) Histogram of p40 lateral diffusion coefficients for particles that diffuse at least 20 frames ( $n=716$ , three cells) with mean diffusion coefficient of  $0.63 \pm 0.05 \mu\text{m}^2/\text{second}$ . An example is shown in supplementary material Movie 10. (B) Lifetime distribution of diffusing p40 molecules ( $n=8325$ , three cells). Single exponential fit of 1-CF (not shown) gives a mean lifetime of  $325 \pm 17$  mseconds. (C) Trajectory of a p40-EGFP molecule that laterally diffuses before transitioning to retrograde flow (corresponds to supplementary material Movie 10). Orange section of the track indicates diffusion, and maroon section indicates retrograde flow. Camera exposures occur at fast 10 frames per second (f.p.s.) imaging conditions. (D) Trajectory of a p40-EGFP molecule that undergoes retrograde motion without any prior diffusion (corresponds to supplementary material Movie 11). Exposures are 10 f.p.s. (E) Selected images from supplementary material Movie 12, which shows diffusion of a p40-EGFP molecule (first five frames, orange tracks, 10 f.p.s. imaging conditions), then retrograde motion (next five frames, maroon tracks, 10 f.p.s. imaging conditions), and then retrograde motion with 0.33 f.p.s. imaging conditions (final six frames, red tracks). The slower imaging mode is better able to capture retrograde motion. Dashed line indicates cell edge. Scale bars:  $1 \mu\text{m}$ . (F) Trajectory of the p40-EGFP molecule in E. Orange section of the track shows diffusion at 10 f.p.s., maroon section indicates retrograde flow at 10 f.p.s., and red section shows retrograde flow at 0.33 f.p.s. imaging frequency (left). MSD versus time plot shows that this particle has a lateral diffusion coefficient of  $0.12 \mu\text{m}^2/\text{second}$  (right).

of time. With this approach, we could capture molecules transitioning from rapid diffusion to an extended period of retrograde movement. In Fig. 6E and supplementary material

Movie 12, we show a molecule of p40-EGFP, which underwent 400 mseconds of lateral diffusion with a diffusion coefficient of  $0.12 \mu\text{m}^2/\text{second}$  (Fig. 6F, right) before its incorporation into the cytoskeletal network. We then followed the molecule during its retrograde motion in a lower-frequency imaging mode. This method enabled us to visualize retrograde flow after particle diffusion (Fig. 6F, left). We found 13 p40 molecules that showed clear retrograde flow. Four of these molecules were preceded by at least four frames (400 mseconds) of lateral diffusion. The other molecules underwent retrograde flow without detectable lateral diffusion, or diffusion was too brief for us to observe. Together, these data show that some Arp2/3 complexes locally search the membrane by 2D diffusion for short periods whereas other molecules are recruited directly from the cytosol before incorporation into the cytoskeleton.

## Discussion

We uncovered new behavior of SCAR/WAVE and Arp2/3 complexes with single-molecule imaging before, during and after nucleation in cells. These data are summarized in our model (Fig. 7). Our first insight relates to the order of recruitment of SCAR/WAVE and Arp2/3 complexes to the plasma membrane. Actin nucleation is a highly regulated event that requires the convergence of several intracellular signals and cytoskeletal structures. Activation of the Arp2/3 complex requires its interaction with nucleation-promoting factors such as the SCAR/WAVE complex, as well as actin filaments (Mullins et al., 1998; Machesky et al., 1999). Similarly, SCAR/WAVE complex activation requires the combinatorial input of Rac-GTP, phosphoinositides and other signals (Oikawa et al., 2004; Lebensohn and Kirschner, 2009; Chen et al., 2010). Two models have been proposed for how the SCAR/WAVE and Arp2/3 complexes first associate with the membrane. In the first model, the SCAR/WAVE complex is recruited and activated by plasma-membrane-bound components such as Rac-GTP and phosphoinositides, and then the Arp2/3 complex is recruited from the cytosol to this membrane-bound SCAR/WAVE complex (Lebensohn and Kirschner, 2009; Chen et al., 2010). In the second model, the Arp2/3 complex is pre-associated with the SCAR/WAVE complex in the cytosol, and both of these complexes are recruited together to membranes (Stradal et al., 2004). However, WAVE2 and p40 have different distributions on the membrane (Figs 1, 2), which suggests that not every SCAR/WAVE complex is pre-associated with an Arp2/3 complex.

What happens after the SCAR/WAVE complex initially associates with the plasma membrane by binding to Rac-GTP or phosphoinositides? The SCAR/WAVE complex probably recruits the Arp2/3 complex to the plasma membrane, as reflected in the similar lifetime of p40 and WAVE2 on the membrane (Fig. 5C, Fig. 6B). Both WAVE2 and p40 laterally diffuse upon recruitment to the plasma membrane, probably because of Rac-GTP or phospholipid binding. Rac2 has a diffusion coefficient of  $0.54 \pm 0.04 \mu\text{m}^2/\text{second}$  (supplementary material Fig. S3A,B); the diffusion coefficient for WAVE2 is  $0.41 \pm 0.04 \mu\text{m}^2/\text{second}$  (Fig. 5B); and the diffusion coefficient for p40 is  $0.63 \pm 0.05 \mu\text{m}^2/\text{second}$  (Fig. 6A). These values are within the expected range of diffusion coefficients for membrane-associated proteins (Murakoshi et al., 2004; Lommerse et al., 2004; Douglass and Vale, 2005; Matsuoka et al., 2006). Lateral diffusion of SCAR/WAVE and Arp2/3 complexes could help these proteins perform a constrained 2D search for nucleation binding sites, including actin

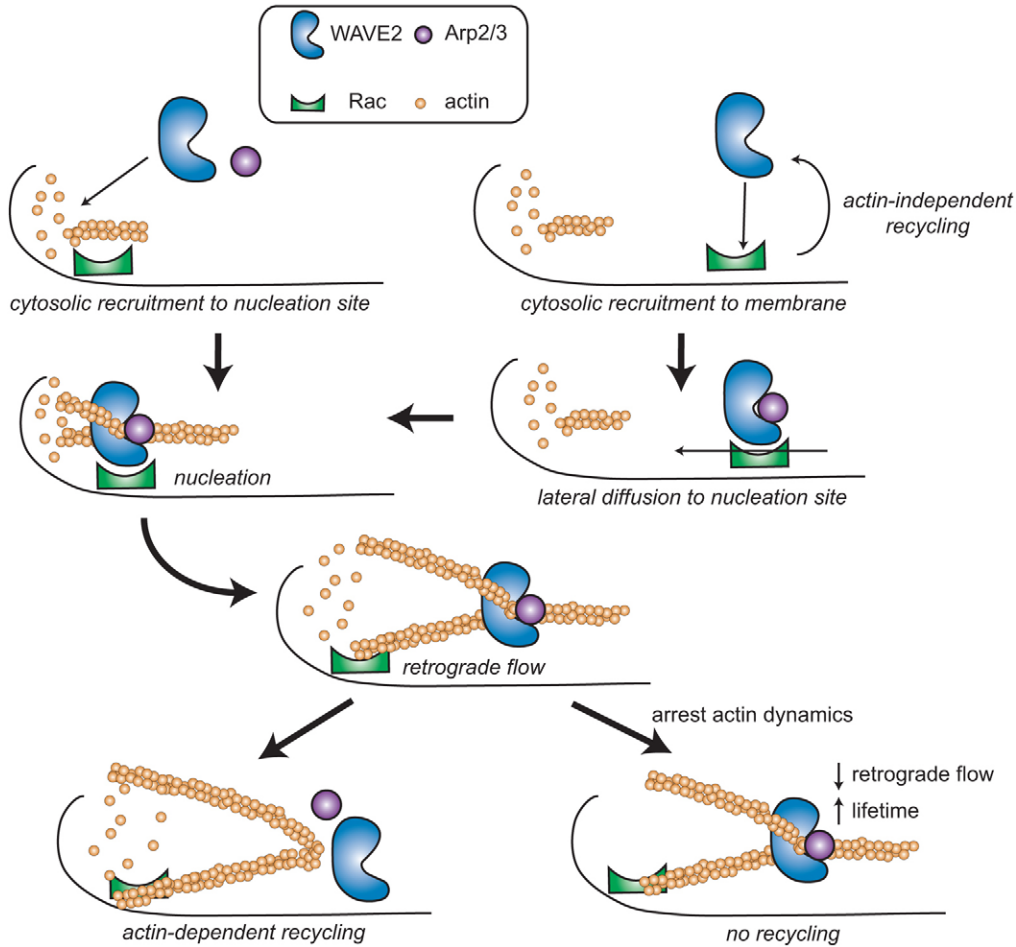


**Fig. 7. Model for SCAR/WAVE-mediated actin nucleation in cells.** SCAR/WAVE and Arp2/3 complexes have two modes of recruitment to nucleation sites: through cytosol recruitment or through membrane-bound lateral diffusion. Diffusing molecules of the SCAR/WAVE complex can release from the membrane independently of actin nucleation. Once a SCAR/WAVE complex integrates into the actin meshwork after nucleation, recycling occurs through actin-based retrograde flow.

barbed ends or sides of filaments, which are necessary to co-activate the Arp2/3 complex. Limited dimensionality searches have been reported in other biological contexts to decrease search time. For instance, the LacI repressor executes short 1D searches along DNA to find its *lacO* target 100 times faster than can be accomplished with 3D diffusion in the cytosol (Riggs et al., 1970; von Hippel and Berg, 1989; Wang et al., 2006; Elf et al., 2007). These constrained diffusion events need not be extensive to dramatically decrease search time; the LacI repressor spends 90% of the time diffusing on DNA with a short residence time of 5 mseconds (Elf et al., 2007). Both WAVE2 and p40 had similar residence times of  $\sim 300$  mseconds during lateral diffusion (Fig. 5C and Fig. 6B), and more rapid imaging as described previously (Elf et al., 2007) might be needed to capture very short-lived 2D searches.

What happens after SCAR/WAVE and Arp2/3 complexes trigger an actin-nucleation event? We show that the Arp2/3 complex incorporates into the actin network and undergoes retrograde flow, which is consistent with previous reports (Ponti et al., 2004; Miyoshi et al., 2006; Iwasa and Mullins, 2007). Surprisingly, we also observed retrograde flow of the SCAR/WAVE complex (Fig. 1). Because WAVE2 retrograde speed and lifetime matches that of actin and p40 (Fig. 2), we hypothesize that WAVE2 incorporates into the actin meshwork after a nucleation event. Alternatively, WAVE2 might bind the side of an actin

filament without first activating Arp2/3 to undergo retrograde motion. In support of the former model, most WAVE2 molecules with retrograde motion first attach to the actin network near the leading edge, where the SCAR/WAVE complex activates the Arp2/3 complex. However, the frequency of WAVE2 retrograde flow is significantly lower than either actin or p40 (Fig. 1F). Several possibilities could account for the discrepancy between the SCAR/WAVE and Arp2/3 complexes. The simplest hypothesis is that only a subset of membrane-bound SCAR/WAVE complex is involved in Arp2/3 complex recruitment and actin nucleation. Consistent with this hypothesis, the overall distributions of WAVE2 and p40 differ, with the cell periphery more enriched for the SCAR/WAVE complex (Fig. 1A) compared with the Arp2/3 complex (Fig. 2A). Alternatively, the SCAR/WAVE complex might activate multiple Arp2/3 molecules before being recycled through retrograde flow. In this scenario, most SCAR/WAVE complexes remain associated at the cell periphery after nucleation and only occasionally track with an Arp2/3 complex during retrograde flow. Finally, all SCAR/WAVE complexes that induce actin nucleation might be removed from the membrane by incorporating into the actin network, but some molecules might be removed more rapidly than our imaging conditions can capture. Future studies are needed to distinguish between these possibilities.

Our work sheds new light on the role of actin polymerization in SCAR/WAVE complex recycling. Both SCAR/WAVE

complex removal from the actin cortex (Weiner et al., 2007; Millius et al., 2009) (this study) and N-WASP removal from the surface of vaccinia viruses (Weisswange et al., 2009) depend on actin polymer. Similarly, regulators of actin assembly in budding yeast require actin polymer for rapid recycling (Kaksonen et al., 2003). For these experiments, actin drugs such as latrunculin have been used to uncover the role of actin polymer in recycling. However, latrunculin not only stops new assembly but also results in disassembly of the existing actin network. This makes it difficult to discern whether ongoing actin assembly or recycling proteins associated with the actin network is more relevant for recycling nucleation-promoting factors. There is evidence that both of these mechanisms participate in recycling endocytic components in yeast. For instance, the actin network is known to serve as a scaffold for proteins such as phosphatidylinositol (4,5)-bisphosphate phosphatases, which catabolize signals required for endocytosis (Sun et al., 2007). By contrast, recycling has also been shown to involve the force of actin polymerization to physically dissociate components from the membrane (Kaksonen et al., 2003). To discriminate which of these mechanisms is responsible for SCAR/WAVE complex recycling, we used a combination of actin drugs to stop new actin assembly while also stabilizing the existing actin cytoskeleton (Peng et al., 2011). This pharmacological cocktail increases the lifetime of the cortical WAVE2 complex (Fig. 4B,C), which suggests that ongoing assembly, and not an actin-network-associated effector protein involved in SCAR/WAVE turnover, is more relevant for SCAR/WAVE recycling. However, inhibition of actin dynamics had little effect on the global pool of WAVE2 (assayed by FRAP, Fig. 4F). This suggests that SCAR/WAVE molecules exist in two distinct states. In the first state, SCAR/WAVE molecules freely associate and dissociate with the plasma membrane independently of actin polymerization. This probably represents a low-affinity interaction of the SCAR/WAVE complex with factors such as Rac and phosphoinositides. In the second state, which represents a small fraction of the total pool (Fig. 1F), molecules undergo actin-dependent retrograde flow, and require actin polymerization for recycling. This probably represents SCAR/WAVE molecules that are associated with the actin cytoskeleton. We favor a model where the SCAR/WAVE complex performs multiple diffusive membrane searches until it integrates into the actin meshwork through Arp2/3 activation, and subsequently recycles through actin-based retrograde flow.

## Materials and Methods

### Plasmids and reagents

Plasmids containing cDNA encoding human  $\beta$ -actin subcloned into pEGFP-C1-derived vector (Clontech Laboratories) or the *Xenopus* p40 subunit of the Arp2/3 complex subcloned into the pEGFP-N1-derived vector containing a defective cytomegalovirus (delCMV) have been previously published (Watanabe and Mitchison, 2002; Miyoshi et al., 2006). EST clone of *Xenopus* WAVE2 was obtained from the IMAGE consortium and subcloned into the pEGFP-N1 delCMV vector. Human Rac2-GFP (Michaelson et al., 2001) and RacN17 (Srinivasan et al., 2003) have been described previously. Y27632 (Calbiochem) was incubated with cells at final concentration of 10  $\mu$ M for at least 30 minutes before imaging. Jasplakinolide (Calbiochem) and latrunculin (Calbiochem) were prepared at 2  $\times$  final concentration (40  $\mu$ M) and acutely added during imaging. XTC cells were cultured and transfected as described previously (Watanabe and Mitchison, 2002).

### Single-molecule microscopy

Single-molecule imaging was performed as previously described (Watanabe and Mitchison, 2002). Images were acquired in Japan and in the USA on a variety of different microscopes (BX52 or IX71; Olympus; or TI-2000, Nikon) with different EM-CCD cameras (MMX 1300-YHS, CoolSNAP HQ, Photometrics Evolve,

Photometrics Cascade II:512, or Andor), acquisition software (Metamorph or NIS-Elements), lamps (100 W mercury or 75 W Xenon), lasers (20 mW, BCD1 Melles Griot or 100 mW, LMM5 Spectral Research) and objectives (planApo 100  $\times$  objective; NA 1.40 oil, Olympus or NA 1.49 oil, Nikon). Data from all microscope set-ups were comparable and indicate the robustness of the observed phenomena. XTC cells were plated on polylysine-coated coverglass for 20 minutes in 70% Leibovitz's L-15 medium (Invitrogen) without serum. Time-lapse imaging was performed at 21–23  $^{\circ}$ C up to 3 hours after cells were seeded. Epifluorescence microscopy imaging of retrograde flow was performed with a 2  $\times$  lens inserted for cells expressing a low concentration of EGFP-tagged proteins with 2–3 second exposures every 3 seconds. Neutral density filters were used to reduce illumination intensity so that fluorescence decay caused by photobleaching was minimized. The field diaphragm was closed to restrict illumination to the cell edge and diminish out-of-focus light from the cell body. Diffusing molecules were observed by illuminating for 40–100 mseconds in total internal reflection fluorescence (TIRF) microscopy for  $\sim$ 100 frames.

### FRAP imaging

Plated cells were imaged with a 488 laser line in TIRF microscopy for 400–600 mseconds every 4–6 seconds for 30–60 seconds, a 1 second 488 FRAP pulse with full laser power was spatially controlled and applied using a mosaic digital micromirror device (Andor), and then cells were imaged for 60 seconds to observe fluorescence recovery. Fluorescence intensity was normalized to the fluorescence intensity immediately before (intensity = 1) and immediately after FRAP (intensity = 0).

### Image analysis

Retrograde motion of WAVE2 molecules was analyzed using the two-dimensional Gaussian fit method over a 5  $\times$  5 pixel region of interest with GTrack software (G-Angstrom, Sendai, Japan). Retrograde motion of p40 and actin molecules was analyzed using GMimPro software (Mashanov and Molloy, 2007). Lifetime measurements were normalized for photobleaching as described (Watanabe and Mitchison, 2002). Mean lifetime ( $\tau$ ) was determined by taking 1-cumulative frequency (CF) and fitting to the curve  $C \exp(-\lambda t)$ , where  $\lambda$  is the first-order dissociation rate and  $C$  is a constant with Prism 5.0 software (Graphpad, San Diego, CA) (Hansen and Mullins, 2010; Bieling et al., 2007). Particle diffusion was measured in Matlab (Mathworks, Natick, MA) with Utrack (Jaqaman et al., 2008). Error bars for mean diffusion coefficients and mean lifetimes are 95% confidence intervals. Diffusion constants did not vary significantly between the cell periphery and the cell interior (supplementary material Fig. S3D,E). Maximum intensity projections and kymographs were created using ImageJ. We used the image calculator from ImageJ to capture molecules transitioning from diffusion to retrograde flow. We created a maximum intensity projection of the last five frames in the fast imaging mode before switching to the slower imaging mode. This maximum intensity projection highlights stabilized particles that might subsequently undergo retrograde flow and eliminates diffusing particles. Then we created a maximum intensity projection from five frames earlier in the imaging acquisition. We subtracted these two maximum intensity projections. Most stabilized molecules appear in both maximum intensity projections and thus are eliminated in the subtracted image. However, a few spots remain, which suggests that they were stabilized particles in the maximum intensity projection just prior to switching imaging modes, but not a stabilized particle earlier in the imaging acquisition. These molecules were subsequently analyzed for diffusion and retrograde flow with Utrack in Matlab.

### Reducing photodamage on actin retrograde speed

Single-molecule imaging can only be performed at low concentrations of fluorescent protein where the individual fluorophores are well separated. We compared two different strategies for achieving low fluorescent protein concentration. One approach uses high-intensity light to bleach cells expressing moderate or high amounts of fluorescent proteins down to concentrations that are compatible with single-molecule imaging (de Keijzer et al., 2008; van Hemert et al., 2010). When we analyzed XTC cells expressing low levels of the p40 subunit of the Arp2/3 complex under both high- and low-intensity light (supplementary material Fig. S4, 0.11 and 1.8 mW, respectively) we found that, as expected, the higher-intensity light exponentially increased photobleaching (supplementary material Fig. S4C). However, the brighter light also dramatically reduced mean retrograde speed of p40 (supplementary material Fig. S4B,D), suggesting that bleaching cells down to single-molecule levels is unsuitable for analyzing actin dynamics. Instead, we used a crippled CMV promoter to transcriptionally limit expression of fluorescent proteins, thereby achieving low concentrations of fluorescent proteins without the need for photobleaching (Watanabe and Mitchison, 2002). This avoids potential artifacts from overexpression (Riedl et al., 2008) and eliminates the photodamaging effects of photobleaching on actin dynamics.

## Acknowledgements

We thank members of the Weiner and Watanabe labs for helpful discussions, constructive criticisms, and technical support. Rac2 and RacN17 plasmids were kind gifts from Henry Bourne. Purified monomeric GFP was a kind gift from Scott Hansen.

## Funding

A.M. was supported by the JSPS and National Science Foundation EAPSI Fellowship; N.W. was supported by the Funding Program for Next Generation of World-Leading Researchers; and O.D.W. was supported by the National Institutes of Health [grant number R01 GM084040]. Deposited in PMC for release after 12 months.

Supplementary material available online at

<http://jcs.biologists.org/lookup/suppl/doi:10.1242/jcs.091157/-/DC1>

## References

- Bear, J. E., Rawls, J. F. and Saxe, C. L. (1998). SCAR, a WASP-related protein, isolated as a suppressor of receptor defects in late Dictyostelium development. *J. Cell Biol.* **142**, 1325-1335.
- Bieling, P., Laan, L., Schek, H., Munteanu, E. L., Sandblad, L., Dogterom, M., Brunner, D. and Surrey, T. (2007). Reconstitution of a microtubule plus-end tracking system in vitro. *Nature* **450**, 1100-1105.
- Chen, Z., Borek, D., Padrick, S. B., Gomez, T. S., Metlagel, Z., Ismail, A. M., Umetani, J., Billadeau, D. D., Otwinowski, Z. and Rosen, M. K. (2010). Structure and control of the actin regulatory WAVE complex. *Nature* **468**, 533-538.
- Cramer, L. P. and Mitchison, T. J. (1997). Investigation of the mechanism of retraction of the cell margin and rearward flow of nodules during mitotic cell rounding. *Mol. Biol. Cell* **8**, 109-119.
- de Keijzer, S., Serge, A., van Hemert, F., Lommerse, P. H. M., Lamers, G. E. M., Spaik, H. P., Schmidt, T. and Snaar-Jagalska, B. E. (2008). A spatially restricted increase in receptor mobility is involved in directional sensing during Dictyostelium discoideum chemotaxis. *J. Cell Sci.* **121**, 1750-1757.
- Douglass, A. D. and Vale, R. D. (2005). Single-molecule microscopy reveals plasma membrane microdomains created by protein-protein networks that exclude or trap signaling molecules in T cells. *Cell* **121**, 937-950.
- Elf, J., Li, G. W. and Xie, X. S. (2007). Probing transcription factor dynamics at the single-molecule level in a living cell. *Science* **316**, 1191-1194.
- Hahne, P., Sechi, A., Benesch, S. and Small, J. V. (2001). Scar/WAVE is localized at the tips of protruding lamellipodia in living cells. *FEBS Lett.* **492**, 215-220.
- Hansen, S. D. and Mullins, R. D. (2010). VASP is a processive actin polymerase that requires monomeric actin for barbed end association. *J. Cell Biol.* **191**, 571-584.
- Ibarra, N., Blagg, S. L., Vazquez, F. and Insall, R. H. (2006). Nap1 regulates Dictyostelium cell motility and adhesion through SCAR-dependent and -independent pathways. *Curr. Biol.* **16**, 717-722.
- Iwasa, J. H. and Mullins, R. D. (2007). Spatial and temporal relationships between actin-filament nucleation, capping, and disassembly. *Curr. Biol.* **17**, 395-406.
- Jagaman, K., Loerke, D., Metten, M., Kuwata, H., Grinstein, S., Schmid, S. L. and Danuser, G. (2008). Robust single-particle tracking in live-cell time-lapse sequences. *Nat. Methods* **5**, 695-702.
- Kaksonen, M., Sun, Y. and Drubin, D. G. (2003). A pathway for association of receptors, adaptors, and actin during endocytic internalization. *Cell* **115**, 475-487.
- King, J. S., Veltman, D. M., Georgiou, M., Baum, B. and Insall, R. H. (2010). SCAR/WAVE is activated at mitosis and drives myosin-independent cytokinesis. *J. Cell Sci.* **123**, 2246-2255.
- Lai, F. P., Szczydrak, M., Block, J., Faix, J., Breitsprecher, D., Mannherz, H. G., Stradal, T. E., Dunn, G. A., Small, J. V. and Rottner, K. (2008). Arp2/3 complex interactions and actin network turnover in lamellipodia. *EMBO J.* **27**, 982-992.
- Lebensohn, A. M., and Kirschner, M. W. (2009). Activation of the WAVE complex by coincident signals controls actin assembly. *Mol. Cell* **36**, 512-524.
- Lin, C. H. and Forscher, P. (1995). Growth cone advance is inversely proportional to retrograde F-actin flow. *Neuron* **14**, 763-771.
- Lommerse, P. H. M., Blab, G. A., Cognet, L., Harms, G. S., Snaar-Jagalska, B. E., Spaik, H. P. and Schmidt, T. (2004). Single-molecule imaging of the H-ras membrane-anchor reveals domains in the cytoplasmic leaflet of the cell membrane. *Biophys. J.* **86**, 609-616.
- Machesky, L. M. and Insall, R. H. (1998). Scar1 and the related Wiskott-Aldrich syndrome protein, WASP, regulate the actin cytoskeleton through the Arp2/3 complex. *Curr. Biol.* **8**, 1347-1356.
- Machesky, L. M., Mullins, R. D., Higgs, H. N., Kaiser, D. A., Blanchoin, L., May, R. C., Hall, M. E. and Pollard, T. D. (1999). Scar, a WASP-related protein, activates nucleation of actin filaments by the Arp2/3 complex. *Proc. Natl. Acad. Sci. USA* **96**, 3739-3744.
- Mashanov, G. I. and Molloy, J. E. (2007). Automatic detection of single fluorophores in live cells. *Biophys. J.* **92**, 2199-2211.
- Matsuoka, S., Iijima, M., Watanabe, T. M., Kuwayama, H., Yanagida, T., Devreotes, P. N. and Ueda, M. (2006). Single-molecule analysis of chemoattractant-stimulated membrane recruitment of a PH-domain-containing protein. *J. Cell Sci.* **119**, 1071-1079.
- Michaelson, D., Silletti, J., Murphy, G., D'Eustachio, P., Rush, M. and Philips, M. R. (2001). Differential Localization of Rho Gtpases in Live Cells. *J. Cell Biol.* **152**, 111-126.
- Miki, H., Suetsugu, S. and Takenawa, T. (1998). WAVE, a novel WASP-family protein involved in actin reorganization induced by Rac. *EMBO J.* **17**, 6932-6941.
- Millius, A., Dandekar, S. N., Houk, A. R. and Weiner, O. D. (2009). Neutrophils establish rapid and robust WAVE complex polarity in an actin-dependent fashion. *Curr. Biol.* **19**, 253-259.
- Miyoshi, T., Tsuji, T., Higashida, C., Hertzog, M., Fujita, A., Narumiya, S., Scita, G. and Watanabe, N. (2006). Actin turnover-dependent fast dissociation of capping protein in the dendritic nucleation actin network, evidence of frequent filament severing. *J. Cell Biol.* **175**, 947-955.
- Mullins, R. D., Heuser, J. A. and Pollard, T. D. (1998). The interaction of Arp2/3 complex with actin, nucleation, high affinity pointed end capping, and formation of branching networks of filaments. *Proc. Natl. Acad. Sci. USA* **95**, 6181-6186.
- Murakoshi, H., Iino, R., Kobayashi, T., Fujiwara, T., Ohshima, C., Yoshimura, A. and Kusumi, A. (2004). Single-molecule imaging analysis of Ras activation in living cells. *Proc. Natl. Acad. Sci. USA* **101**, 7317-7322.
- Oikawa, T., Yamaguchi, H., Itoh, T., Kato, M., Ijuin, T., Yamazaki, D., Suetsugu, S. and Takenawa, T. (2004). PtdIns(3,4,5)P<sub>3</sub> binding is necessary for WAVE2-induced formation of lamellipodia. *Nat. Cell Biol.* **6**, 420-426.
- Padrick, S. B. and Rosen, M. K. (2010). Physical mechanisms of signal integration by WASP family proteins. *Annu. Rev. Biochem.* **79**, 707-735.
- Patel, F. B., Bernadskaya, Y. Y., Chen, E., Jobanputra, A., Pooladi, Z., Freeman, K. L., Gally, C., Mohler, W. A. and Soto, M. C. (2008). The WAVE/SCAR complex promotes polarized cell movements and actin enrichment in epithelia during C. elegans embryogenesis. *Dev. Biol.* **324**, 297-309.
- Peng, G. E., Wilson, S. R. and Weiner, O. D. (2011). A pharmacological cocktail for arresting actin dynamics in living cells. *Mol. Biol. Cell* **21**, 3986-3994.
- Ponti, A., Machacek, M., Gupton, S. L., Waterman-Storer, C. M. and Danuser, G. (2004). Two distinct actin networks drive the protrusion of migrating cells. *Science* **305**, 1782-1786.
- Ponti, A., Matov, A., Adams, M., Gupton, S., Waterman-Storer, C. M. and Danuser, G. (2005). Periodic patterns of actin turnover in lamellipodia and lamellae of migrating epithelial cells analyzed by quantitative Fluorescent Speckle Microscopy. *Biophys. J.* **89**, 3456-3469.
- Renkawitz, J., Schumann, K., Weber, M., Lämmermann, T., Pflücke, H., Piel, M., Polleux, J., Spatz, J. P. and Sixt, M. (2009). Adaptive force transmission in amoeboid cell migration. *Nat. Cell Biol.* **11**, 1438-1443.
- Riedl, J., Crevenna, A. H., Kessenbrock, K., Yu, J. H., Neukirchen, D., Bista, M., Bradke, F., Jenne, D., Holak, T. A., Werb, Z., Sixt, M. and Wedlich-Soldner, R. (2008). Lifeact, a versatile marker to visualize F-actin. *Nat. Methods* **5**, 605-607.
- Riggs, A. D., Bourgeois, S. and Cohn, M. (1970). The lac repressor-operator interaction. 3. Kinetic studies. *J. Mol. Biol.* **53**, 401-417.
- Rogers, S. L., Wiedemann, U., Sturman, N. and Vale, R. D. (2003). Molecular requirements for actin-based lamella formation in *Drosophila* S2 cells. *J. Cell Biol.* **162**, 1079-1088.
- Rohatgi, R., Ma, L., Miki, H., Lopez, M., Kirchhausen, T., Takenawa, T. and Kirschner, M. W. (1999). The interaction between N-WASP and the Arp2/3 complex links Cdc42-dependent signals to actin assembly. *Cell* **97**, 221-231.
- Srinivasan, S., Wang, F., Glavas, S., Ott, A., Hofmann, F., Aktories, K., Kalman, D. and Bourne, H. R. (2003). Rac and Cdc42 play distinct roles in regulating PI(3,4,5)P<sub>3</sub> and polarity during neutrophil chemotaxis. *J. Cell Biol.* **160**, 375-385.
- Steffen, A., Rottner, K., Ehinger, J., Innocenti, M., Scita, G., Wehland, J. and Stradal, T. E. B. (2004). Sra-1 and Nap1 link Rac to actin assembly driving lamellipodia formation. *EMBO J.* **23**, 749-759.
- Stradal, T., Courtney, K. D., Rottner, K., Hahne, P., Small, J. V. and Pendergast, A. M. (2001). The Abl interactor proteins localize to sites of actin polymerization at the tips of lamellipodia and filopodia. *Curr. Biol.* **11**, 891-895.
- Stradal, T. E. B., Rottner, K., Disanza, A., Confalonieri, S., Innocenti, M. and Scita, G. (2004). Regulation of actin dynamics by WASP and WAVE family proteins. *Trends Cell Biol.* **14**, 303-311.
- Sun, Y., Carroll, S., Kaksonen, M., Toshima, J. Y. and Drubin, D. G. (2007). PtdIns(4,5)P<sub>2</sub> turnover is required for multiple stages during clathrin- and actin-dependent endocytic internalization. *J. Cell Biol.* **177**, 355-367.
- Theriot, J. A. and Mitchison, T. J. (1991). Actin microfilament dynamics in locomoting cells. *Nature* **352**, 126-131.
- Theriot, J. A. and Mitchison, T. J. (1992). Comparison of actin and cell surface dynamics in motile fibroblasts. *J. Cell Biol.* **119**, 367-377.
- van Hemert, F., Lazova, M. D., Snaar-Jagaska, B. E. and Schmidt, T. (2010). Mobility of G proteins is heterogeneous and polarized during chemotaxis. *J. Cell Sci.* **123**, 2922-2930.
- von Hippel, P. H. and Berg, O. G. (1989). Facilitated target location in biological systems. *J. Biol. Chem.* **264**, 675-678.
- Wang, Y. L. (1985). Exchange of actin subunits at the leading edge of living fibroblasts, possible role of treadmilling. *J. Cell Biol.* **101**, 597-602.
- Wang, Y. M., Austin, R. H. and Cox, E. C. (2006). Single molecule measurements of repressor protein 1D diffusion on DNA. *Phys. Rev. Lett.* **97**, 048302.
- Watanabe, N. and Mitchison, T. J. (2002). Single-molecule speckle analysis of actin filament turnover in lamellipodia. *Science* **295**, 1083-1086.

- Weiner, O. D., Rentel, M. C., Ott, A., Brown, G. E., Jedrychowski, M., Yaffe, M. B., Gygi, S. P., Cantley, L. C., Bourne, H. R. and Kirschner, M. W. (2006). Hem-1 complexes are essential for Rac activation, actin polymerization, and myosin regulation during neutrophil chemotaxis. *PLoS Biol.* **4**, e38.
- Weiner, O. D., Marganski, W. A., Wu, L. F., Altschuler, S. J. and Kirschner, M. W. (2007). An actin-based wave generator organizes cell motility. *PLoS Biol.* **5**, e221.
- Weisswange, I., Newsome, T. P., Schleich, S. and Way, M. (2009). The rate of N-WASP exchange limits the extent of ARP2/3-complex-dependent actin-based motility. *Nature* **458**, 87-91.
- Xiong, Y., Huang, C. H., Iglesias, P. A. and Devreotes, P. N. (2010). Cells navigate with a local-excitation, global-inhibition-biased excitable network. *Proc. Natl. Acad. Sci. USA* **107**, 17079-17086.
- Yan, C., Martinez-Quiles, N., Eden, S., Shibata, T., Takeshima, F., Shinkura, R., Fujiwara, Y., Bronson, R., Snapper, S. B., Kirschner, M. W., Geha, R., Rosen, F. S. and Alt, F. W. (2003). WAVE2 deficiency reveals distinct roles in embryogenesis and Rac-mediated actin-based motility. *EMBO J.* **22**, 3602-3612.
- Zallen, J. A., Cohen, Y., Hudson, A. M., Cooley, L., Wieschaus, E. and Schejter, E. D. (2002). SCAR is a primary regulator of Arp2/3-dependent morphological events in *Drosophila*. *J. Cell Biol.* **156**, 689-701.